

per mil (1σ). In an effort to reduce intracoral variability we only sampled the upward-growing portion of coral fronds. To test the variability of our $\delta^{18}\text{O}$ measurements we sampled individual transects from the upper surface all the way around to the shaded or bottom side. No significant $\delta^{18}\text{O}$ differences were found even though there was a reduction in extension rate from the upper to bottom surface of greater than 50%.

20. $\Delta\delta^{18}\text{O} = \delta^{18}\text{O}_m - \delta^{18}\text{O}_{\text{present}} - 0.011\text{UpZ}$, where $\delta^{18}\text{O}_m$ is the measured value of paleosamples, $\delta^{18}\text{O}_{\text{present}}$ is the value of recent *A. palmata* collected from Barbados, UpZ is the uplift corrected depth using Th/U years, and 0.011 is the maximum ice volume-sea level relationship (18). $\Delta T = \Delta\delta^{18}\text{O} \cdot \partial T/\partial\delta^{18}\text{O}$, where $\Delta\delta^{18}\text{O}$ is as defined previously and $\partial T/\partial\delta^{18}\text{O}$ is the temperature-dependent oxygen isotopic fractionation, which is 0.21 per mil per degree Celsius for *Acroporids* (35).
21. Two individual transects encompassing 2 to 4 years of growth from the upward-growing portion of coral fronds, identical to those used in the $\delta^{18}\text{O}$ analyses, were prepared as follows. Samples, approximately 100 to 200 μg , were directly dissolved in a $^{84}\text{Sr}\text{-}^{43}\text{Ca}$ acid spike solution. One microliter of the solution was then loaded onto degassed W filaments and analyzed on a VG Sector Thermal Ionization Mass Spectrometer in static faraday mode. In determining the Sr concentration 120 ratios were measured whereas 150 ratios were measured for Ca. Mass fractionation correction during analysis assumed a natural $^{86}\text{Sr}/^{88}\text{Sr} = 0.1194$ (36), and $^{42}\text{Ca}/^{44}\text{Ca} = 0.31221$ (37).
22. M. R. Palmer and J. M. Edmond, *Earth Planet. Sci. Lett.* **92**, 11 (1989).
23. W. S. Broecker and T. H. Peng, *Tracers in the Sea* (ELDIGIO Press, Columbia University, Palisades, NY, 1982).
24. J. D. Wright, R. G. Fairbanks, J. L. Rubenstone, in preparation.
25. The average linear extension rate of the specimens analyzed was 5.3 ± 1.8 mm as determined from x-radiographs and high-low density pairs (38).
26. S. Levitus, *Climatological Atlas of the World Ocean* (NOAA Prof. Pap. 13, National Oceanic and Atmospheric Administration, Rockville, MD, 1982).
27. J. W. Wells and D. Hill, in *Treatise of Invertebrate Paleontology, part F, Coelenterata*, R. C. Moore, Ed. (Univ. of Kansas and Geological Society of America Press, Lawrence, KS, 1956). In (11) it was stated that preliminary work on *Acroporids* found Sr/Ca ratios similar to those of *M. verrucosa*. $\Delta T^* = [(\text{Sr}/\text{Ca})_m - (\text{Sr}/\text{Ca})_{\text{present}}] \partial T/\partial(\text{Sr}/\text{Ca})$, where $(\text{Sr}/\text{Ca})_{\text{present}}$ is the Sr/Ca ratio of present samples, $(\text{Sr}/\text{Ca})_m$ is for the paleosamples, and $\partial T/\partial(\text{Sr}/\text{Ca})$ is the temperature relation from (11).
28. A. C. Mix, W. F. Ruddiman, A. McIntyre, *Paleoceanography* **1**, 43 (1986); *ibid.*, p. 339.
29. A. C. Ravelo, R. G. Fairbanks, S. G. H. Philander, *ibid.* **5**, 409 (1990).
30. V. Ramanathan *et al.*, *Science* **243**, 57 (1989).
31. E. F. Harrison *et al.*, *J. Geophys. Res.* **95**, 18687 (1990); M. Rieland and R. Stuhlmann, *J. Appl. Meteorology* **32**, 825 (1993).
32. H. Flohn *et al.*, *Climate Dyn.* **4**, 237 (1990); D. Rind *et al.*, *Nature* **349**, 500 (1991).
33. J. B. Pollack *et al.*, *J. Climate* **6**, 1719 (1993).
34. D. Rind, D. W. B. Rossow, *J. Atm. Sci.* **41**, 479 (1984).
35. In (10) no correction for the isotopic composition of surface water was made. We have digitized their data and normalized to 0.0 per mil (SMOW) at 34.31 per mil salinity using annual average salinity (26) and the observed 0.53 relation between $\delta^{18}\text{O}$ and salinity from Pacific GEOSECS stations (39), converting the normalization to the PDB scale. The resulting $\delta^{18}\text{O}_{\text{coral}}$ -temperature relation is 0.21 per mil per degree Celsius.
36. A. O. Nier, *Phys. Rev.* **54**, 275 (1938).
37. W. A. Rüssel *et al.*, *Geochim. Cosmochim. Acta.* **42**, 1075 (1978).
38. R. W. Buddemeir, in *Proceedings of the Second*

- International Coral Reef Symposium 2, Great Barrier Reef Committee, A. M. Cameron et al.*, Eds. (Brisbane, Australia, 1974), pp. 259-267; R. C. Highsmith, *J. Exp. Mar. Biol. Ecol.* **37**, 105 (1979).
39. H. G. Ostlund *et al.*, *GEOSECS Atlantic, Pacific, and Indian Ocean Expeditions*, vol. 7 (National Science Foundation, Washington, DC, 1987).
40. This manuscript benefitted greatly from com-

ments and reviews provided by D. Rind, C. Charles, M. Bender, and an anonymous reviewer. This project has been supported by NSF grants ATM90-01139 and ATM 92-17555 to R.G.F. This is Lamont-Doherty Earth Observatory contribution no. 5166.

26 October 1993; accepted 28 December 1993

Lake-Atmosphere Feedbacks Associated with Paleolakes Bonneville and Lahontan

S. W. Hostetler, F. Giorgi, G. T. Bates, P. J. Bartlein

A high-resolution, regional climate model nested within a general circulation model was used to study the interactions between the atmosphere and the large Pleistocene lakes in the Great Basin of the United States. Simulations for January and July 18,000 years ago indicate that moisture provided by synoptic-scale atmospheric circulation features was the primary component of the hydrologic budgets of Lakes Lahontan and Bonneville. In addition, lake-generated precipitation was a substantial component of the hydrologic budget of Lake Bonneville at that time. This local lake-atmosphere interaction may help explain differences in the relative sizes of these lakes 18,000 years ago.

At the last glacial maximum 18,000 years ago (18 ka), paleolakes Bonneville and Lahontan existed in the Great Basin of the western United States (Fig. 1). The surface area of Lake Bonneville (47,800 km²) was about eight times that of the present Great Salt Lake (6200 km²), and the surface area of Lake Lahontan (14,700 km²) was about six times that of the present lakes in the Lahontan basin (2500 km²) (1-3). Lake-level chronologies (2) indicate that at 18 ka the surface area of Lake Bonneville was nearly as large as the postglacial maximum that occurred at ~14.5 ka, whereas the surface area of Lake Lahontan was about two-thirds of its postglacial maximum, which was at 13.5 ka.

The presence of these lakes from 30 to 12 ka has been linked to atmospheric circulation changes, in particular changes in the mean position of the polar jet stream and associated storm track (4, 5). Simulations with general circulation models (GCMs) have shown that the jet stream was split by the Laurentide Ice Sheet, with the southern branch of the jet displaced to the south (6-9). Hydrological modeling (10) of the Lahontan basin showed that variations of lake levels were consistent with the regional climatic response to these circulation changes. The large sizes of lakes Bonneville and Lahontan suggest that lake-atmosphere interactions (thermal effects and evaporation) within the lake basins

may have generated or enhanced precipitation (5, 11, 12); thus, to some extent, the large lakes may have been self-maintaining.

To investigate the hierarchy of controls of the pluvial climates of the western United States, we used a regional climate model (RegCM) (13, 14). Coastlines and mountainous terrain that exert substantial forcings on the climate of the region were resolved in this model (15). An interactive lake model that can simulate lake temperature, evaporation, and ice cover was also included (16). We conducted a series of 90-day simulations with RegCM to describe the climate of 18 ka and to separate large-scale circulation changes from small-scale lake-atmosphere feedbacks. The simulations were conducted for perpetual January and July conditions; initial and lateral

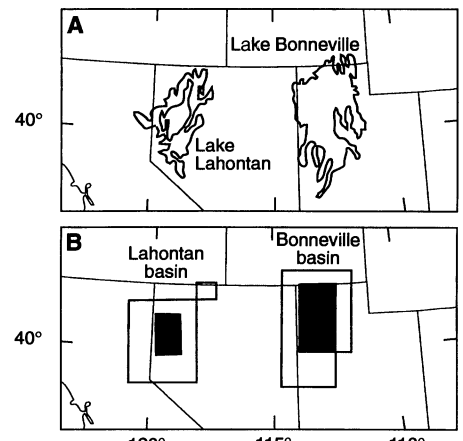


Fig. 1. (A) Locations and sizes of lakes Lahontan and Bonneville. Lake extents are for maximum lake sizes. (B) Model representation of the 18-ka lake surface areas and the lake basins.

S. W. Hostetler, U.S. Geological Survey, 3215 Marine Street, Boulder, CO 80303.
 F. Giorgi and G. T. Bates, National Center for Atmospheric Research, Post Office Box 3000, Boulder, CO 80303.
 P. J. Bartlein, Department of Geography, University of Oregon, Eugene, OR 97403.

boundary conditions were from general circulation model simulations of the climate of 18 ka (7, 17). We used estimates of vegetation type and distribution at 18 ka and the areal coverage of montane glaciers and the Laurentide Ice Sheet to set surface boundary conditions in RegCM. The approximate location, surface areas, and depths of lakes Bonneville and Lahontan also were prescribed in a domain 3000 by 3000 km, centered over the western United States. A resolution of 60 km was used for the simulations (Fig. 1).

To evaluate the model over the basins of interest, we compared (Table 1) precipitation and surface air temperature from present-day January and July simulations with 30-year averages of observations (18). When driven by the GCM, RegCM output was in close agreement with observed precipitation and surface air temperature. The January-July contrasts in precipitation and temperature over both basins were captured, although the simulated January precipitation over the Bonneville basin was somewhat higher than that observed over the Lahontan basin. The Lahontan basin lies in the lee (rain shadow) of the Sierra Nevada, and the overprediction of precipitation in the Lahontan basin may result from smoothing of the actual topography

that occurs in the model at a resolution of 60 km (19).

In the January simulations for 18 ka, the shallow parts of both lakes (4 of 6 grid points of Lake Lahontan and 9 of 15 grid points of Lake Bonneville) became covered with ice, whereas the deeper areas remained ice-free and water-surface temperatures stabilized at $\sim 4^{\circ}\text{C}$. Surface air temperatures in the vicinity of Lake Bonneville were up to 1.5°C greater than they are at present (Fig. 2A), whereas those in the Lahontan region were slightly lower than those at present (but still warmer than those in adjacent regions). The thermal effect of the lakes on surface air temperature at 18 ka was substantial (Fig. 2B): the difference in surface air temperature over the Bonneville basin between the simulation with the lakes and that without exceeded 4°C .

The thermal contrast between the lakes and the atmosphere, together with moisture derived from lake evaporation, induced precipitation over both lake basins (Fig. 2C); precipitation in the 18-ka simulation exceeded that for 0 ka by up to 125 mm over Lake Bonneville and by up to 100 mm over Lake Lahontan. A response of similar magnitude was indicated when the lakes were eliminated in the 18-ka January simulation (Fig. 2D). (Precipitation was slightly great-

Table 1. Simulated and observed precipitation and air temperature for the 0-ka control run. The 0-ka model was from the RegCM-GCM simulation; observed values are the composite 30-year averages of six National Oceanic and Atmospheric Administration weather stations selected in each basin. Jan., January; Jul., July.

Basin	Precipitation (mm)		Temperature ($^{\circ}\text{C}$)	
	Jan.	Jul.	Jan.	Jul.
<i>Model</i>				
Lahontan	70	10	-6	17
Bonneville	40	10	-7	18
<i>Observed</i>				
Lahontan	60	10	-2	17
Bonneville	40	20	-5	20

er over the Lahontan basin at 18 ka without the lake because mesoscale circulations induced by the lake deflected westerly winds and transported most of the moisture generated by lake evaporation to the east of the basin.) Over the Bonneville basin, precipitation in the 18-ka simulation that included the lake was slightly less than in the 18-ka simulation without the lake in the southern and western parts of the basin because ice cover stabilized the air masses and thereby suppressed precipitation. The

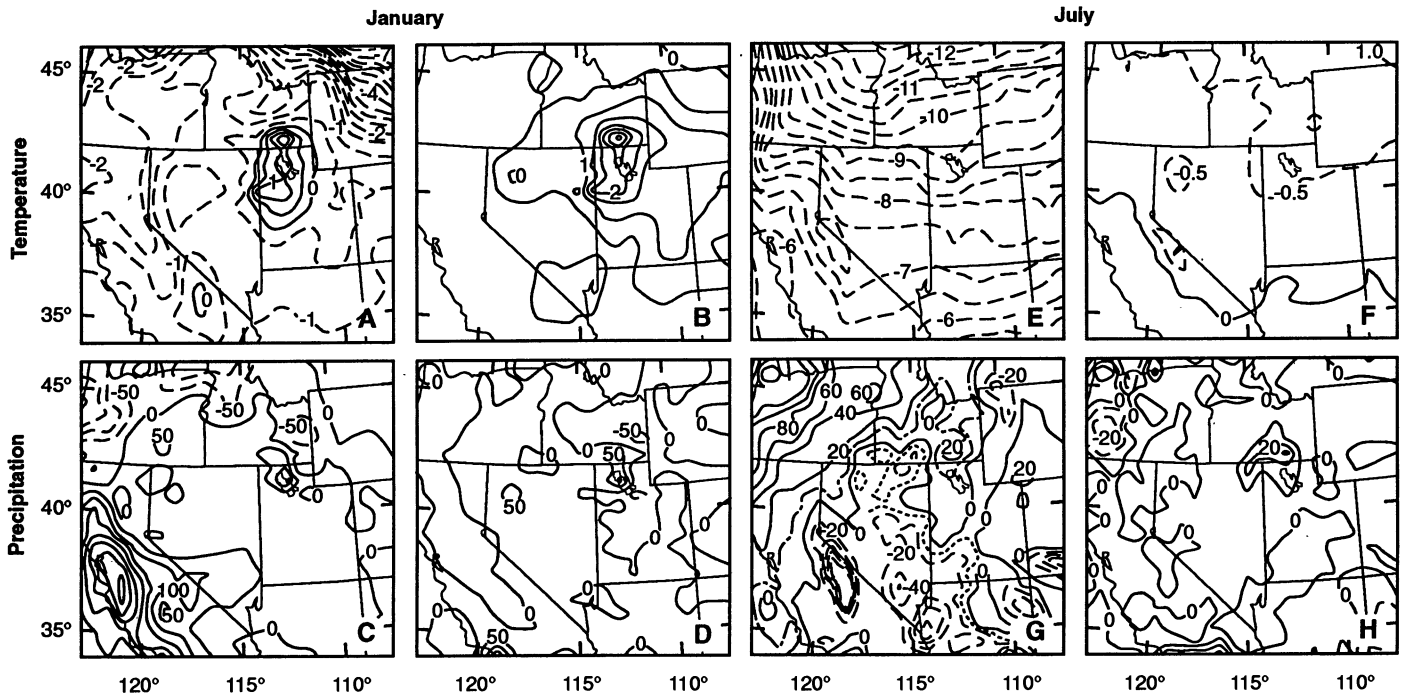


Fig. 2. Comparison of simulation results with and without lakes. (A) January surface air temperature differences; shown are values for 18 ka with the lakes minus the 0-ka contour interval of 0.5°C . (B) January surface air temperature differences; shown are values for 18 ka with the lakes minus values 18 ka without the lakes with a contour interval of 0.5°C . (C) January precipitation differences; shown are values for 18 ka with the lakes minus the 0-ka contour interval of 50 mm. (D) January precipitation differences between the 18 ka simulations with and without the lakes, with a contour interval of 50 mm. (E) July surface air temperature differences;

shown are values for 18 ka with the lakes minus the 0-ka contour interval of 0.5°C . (F) July surface air temperature differences; shown are values for 18 ka with the lakes minus the 18-ka contour interval of 0.5°C . (G) July precipitation differences; shown are values for 18 ka with the lakes minus the 0-ka contour interval of 20 mm. (H) July precipitation differences; shown are values for 18 ka with the lakes minus the 18-ka contour interval (without the lakes) of 10 mm. Temperatures were averaged over the last 60 days of the simulations, and precipitation values are totals for the same period.

Table 2. Model results for simulations with and without lakes 18 ka; control was 0 ka. Precipitation and evaporation values (30-day values) are based on the last 60 simulated days. ΔP , precipitation difference; ΔE , evaporation difference; L.E., lake effect computed as $(\Delta P/\Delta E) E/P$, where E and P represent the evaporation and precipitation in the simulation with both lakes 18 ka. Values are averages over the model grid points representing the lakes and basins; basin values include the lakes.

Formation	Month	$P - E$ (mm)		Lake versus no lake, 18 ka			
		18 ka	0 ka	ΔP (mm)	ΔE (mm)	$\Delta P/\Delta E$	L.E. (%)
Lake Lahontan	January	43	46	9	27	0.3	15
	July	-121	-3	1	121	0.0	0
Lahontan basin	January	79	68	-	9	-	-
	July	-26	-2	0	25	0.0	0
Lake Bonneville	January	45	35	13	23	0.6	23
	July	-95	1	7	99	0.1	59
Bonneville basin	January	43	38	1	14	0.1	3
	July	-41	1	5	43	0.1	38

greater temperature and precipitation response over the Bonneville basin compared to that over the Lahontan basin was a result of a difference in the size of the lakes and the topographic barrier presented by the Wasatch Range, which inhibited the advection of moisture from the basin (20). In addition, precipitation was enhanced by strong, low-level convergence (not apparent in Fig. 2) over the north end of the Bonneville basin, which was induced by the steep temperature gradient between this region and the continental ice to the north.

In the 18-ka July simulations, surface temperatures of both lakes were $\sim 11^\circ\text{C}$ ($\sim 13^\circ\text{C}$ lower than present-day lake temperatures) and the lakes exerted a minor influence on regional air temperature (Fig. 2, E and F) relative to the influence of the large-scale controls. July precipitation was dominated by large-scale circulation features. Precipitation over the Bonneville basin was enhanced relative to the 0-ka simulation (up to 20 mm) by lake-atmosphere feedbacks (Fig. 2G), and relative to the 18-ka simulation that did not include the lakes, precipitation was up to 30 mm greater over the Bonneville basin (Fig. 2H). Lake effects were not associated with Lake Lahontan in either simulation.

The relative contributions of external and internal controls on climate to the hydrologic budgets of the basins can be assessed by comparison of changes in precipitation and evaporation (lake evaporation and land evapotranspiration) and evaporation-precipitation ratios (Table 2) (21). Over the Lahontan basin in the January simulation of 18 ka, net basin moisture [precipitation minus evaporation ($P - E$)] increased by 9 mm (16%) with the lake present, relative to the 0-ka January simulation. Values for $P - E$ for the 18-ka July simulation are lower than those for 0 ka because the presence of the lake increased evaporation from the basin.

In the January simulation, the lake-atmosphere feedbacks generated by Lake Lahontan contributed 15% of the total precipitation in the vicinity of the lake (Table 2); however, in July no effect was indicated around the lake. The basin-wide contribution to precipitation derived from the lake was negligible in both January and July. These results suggest that Lake Lahontan was maintained at its 18-ka size primarily by reduced evaporative losses and enhanced runoff from the higher elevations (Sierra Nevada) of the Lahontan basin that resulted from the southerly displacement of the polar jet stream (5, 10).

For the Bonneville basin at 18 ka, the January $P - E$ value exceeded the control value by 5 mm (13%). As with the Lahontan basin, lake evaporation caused July $P - E$ values for 18 ka to be more negative than 0 ka values. In contrast to that in the Lahontan basin, at 18 ka precipitation in the Bonneville basin generated by the lake was a substantial component of the hydrologic budget (Table 2). Lake-atmosphere feedbacks in January 18 ka contributed 23% of the precipitation in the vicinity of the lake and 3% of the total precipitation over the basin. In July 18 ka, 59% of the precipitation over the lake and 38% of the precipitation over the basin was generated by lake-atmosphere feedbacks. These results indicate that, in addition to the moisture derived from changes in synoptic-scale atmospheric circulation, precipitation generated by lake-atmosphere feedbacks also was important for maintaining the large size of the lake at 18 ka.

Our results indicate that the pluvial climate of the Great Basin was governed by climatic controls that operated both externally to the region (large-scale atmospheric circulation) and internally to the basins (lake-atmosphere feedbacks). The relative contribution by this latter component to the overall pluvial climate strongly depends

on the size and physiographic setting of the lakes. Lake Bonneville, which was larger than Lake Lahontan and was located upwind of a major mountain system, contributed more to its own maintenance than did Lake Lahontan.

REFERENCES AND NOTES

- L. V. Benson *et al.*, *Palaeogeogr. Palaeoclimatol. Palaeoecol.* **78**, 241 (1990). The present-day surface areas of the lakes are reconstructed—that is, the areas that would exist without diversions of river water.
- L. V. Benson, D. M. Currey, Y. Lao, S. W. Hostetler, *ibid.* **95**, 19 (1992).
- D. R. Curry and C. G. Oviatt, in *Problems and Prospects for Predicting Great Salt Lake Levels*, P. A. Kay and H. F. Diaz, Eds. (Center for Public Affairs, University of Utah, 1985), pp. 9–24.
- E. Antevs, *Bull. Univ. Utah Biol. Ser.* **19**, 168 (1948).
- L. V. Benson and R. S. Thompson, in *North America and Adjacent Oceans During the Last Deglaciation*, W. F. Ruddiman and H. E. Wright, Eds. (Geological Society of America, Boulder, CO, 1986), pp. 241–260.
- S. Manabe and A. J. Broccoli, *J. Geophys. Res.* **90**, 2167 (1985).
- J. E. Kutzbach and P. J. Guetter, *J. Atmos. Sci.* **43**, 1726 (1986). The GCM simulations were conducted with version 0 of the National Center for Atmospheric Research Community Climate Model (CCM0).
- D. J. Rind, *J. Geophys. Res.* **92**, 4241 (1987).
- COHMAP Members, *Science* **241**, 1043 (1988).
- S. W. Hostetler and L. V. Benson, *Clim. Dynam.* **4**, 207 (1991).
- W. D. McCoy and L. D. Williams, in *Problems and Prospects for Predicting Great Salt Lake Levels*, P. A. Kay and H. F. Diaz, Eds. (Center for Public Affairs, University of Utah, 1985), pp. 40–53.
- Lake-effect snows around the present-day Great Salt Lake have recently been documented by D. M. Carpenter [*Weather Forecast.* **8**, 181 (1992)].
- RegCM is the climate version of the National Center for Atmospheric Research (NCAR)—Pennsylvania State University mesoscale model MM4. RegCM is a hydrostatic, compressible, primitive equation model written in sigma (σ) coordinates that follow the terrain: $\sigma = (p - p_t)/(p_s - p_t)$ where p is atmospheric pressure, p_t is the pressure at the top of the model, and p_s is surface pressure. For our simulations, p_t was set to 80 mbar and 14 vertical σ levels were used, including five levels below $\sigma = 0.80$, to resolve the planetary boundary layer. The model includes representations of the physics of radiative transfer, cloud, and precipitation processes. A surface-physics package (the Biosphere-Atmosphere Transfer Scheme or BATS [R. E. Dickinson, P. J. Kennedy, A. Henderson-Sellers, M. Wilson, *NCAR Tech. Note, NCAR/TN-275+STR* (1986)]) was used in the model to link the biosphere with the atmosphere. Descriptions of RegCM are given elsewhere (14). A horizontal grid spacing of 60 km was used in this study; typical GCMs use grid spacings of up to 500 km.
- F. Giorgi, G. T. Bates, S. J. Nieman, *J. Climate* **6**, 75 (1993); F. Giorgi, C. Brodeur-Shields, G. T. Bates, *ibid.*, in press.
- R. E. Dickinson, R. M. Errico, F. Giorgi, G. T. Bates, *Climat. Change* **15**, 383 (1986); F. Giorgi and G. T. Bates, *Mon. Weather Rev.* **117**, 2325 (1989).
- S. W. Hostetler and P. J. Bartlein, *Water Resour. Res.* **26**, 2603 (1990); S. W. Hostetler and F. Giorgi, *Clim. Dynam.* **7**, 39 (1992); S. W. Hostetler, G. T. Bates, F. Giorgi, *J. Geophys. Res.* **98**, 5045 (1993); G. T. Bates, F. Giorgi, S. W. Hostetler, *Mon. Weather Rev.* **121**, 1373 (1993).
- Such boundary conditions included (fixed) sea surface temperatures and vertical profiles of atmospheric temperature, wind velocity, and atmospheric mixing ratio along the boundary of the

- model domain. The technique for providing boundary conditions is discussed by F. Giorgi [*J. Climate* 3, 941 (1990)].
18. Neither the Great Salt Lake nor any of the remnant lakes in the Lahontan basin was included in RegCM for the 0-ka simulations because at 60-km resolution the lakes are smaller than the grid in size.
 19. S. W. Hostetler and F. Giorgi, *Water Resour. Res.* 29, 1685 (1993).
 20. These results are consistent with the conclusions of McCoy and Williams (11), who, on the basis of

- modeling the 18-ka size of the Little Cottonwood Canyon Glacier, argued that lake-effect precipitation was a substantial component of the hydrologic budget of the lake.
21. It is customary (2, 9, 10) to quantify change in basin hydrologic budgets in terms of annual $P - E$, but because our results are for perpetual January and July conditions and not for a complete annual cycle, we cannot infer how the annual hydrologic budgets of the lakes may have changed to support the lakes at their 18-ka sizes.

22. We thank J. E. Kutzbach and P. Behling for providing us with GCM history tapes, L. V. Benson for discussions about this research, and D. L. Zahnle for careful reviews of the manuscript. Support for this research was provided by the National Research Program, Water Resources Division of the U.S. Geological Survey (S.W.H.) and by NSF grants to the National Center for Atmospheric Research (F.G. and G.T.B.) and the University of Oregon (P.J.B.).

3 September 1993; accepted 2 December 1993

Mortality Rates in a Genetically Heterogeneous Population of *Caenorhabditis elegans*

Anne Brooks, Gordon J. Lithgow, Thomas E. Johnson*

Age-specific mortality rates in isogenic populations of the nematode *Caenorhabditis elegans* increase exponentially throughout life. In genetically heterogeneous populations, age-specific mortality increases exponentially until about 17 days and then remains constant until the last death occurs at about 60 days. This period of constant age-specific mortality results from genetic heterogeneity. Subpopulations differ in mean life-span, but they all exhibit near exponential, albeit different, rates of increase in age-specific mortality. Thus, much of the observed heterogeneity in mortality rates later in life could result from genetic heterogeneity and not from an inherent effect of aging.

Human mortality rates show a profound relation with chronological age in that mortality increases exponentially with chronological age from 25 to 30 years of age onward (1). Benjamin Gompertz (1825) was the first to recognize this dependency of mortality rate on chronological age and expressed it mathematically by the equation (1, 2)

$$m(t) = Ae^{\alpha t}$$

where $m(t)$ is the mortality rate at time t , A is the mortality rate at reproductive maturity, and α is the Gompertz exponent, which describes the rate of acceleration of age-specific mortality with chronological age. The exact shape of the function describing mortality rates in humans has implications for predictions of demographic trends (3).

Age-specific mortality rates also increase exponentially with chronological age in a variety of other mammals (2, 4) and invertebrates (4). Mortality rate is an exponential function of chronological age in *Caenorhabditis elegans* (5, 6), and the rate of increase of mortality is genetically specified in recombinant-inbred (RI) strains (5, 7). *Age-1* mutant strains also have lower rates of increase of age-specific mortality than wild-type strains (6).

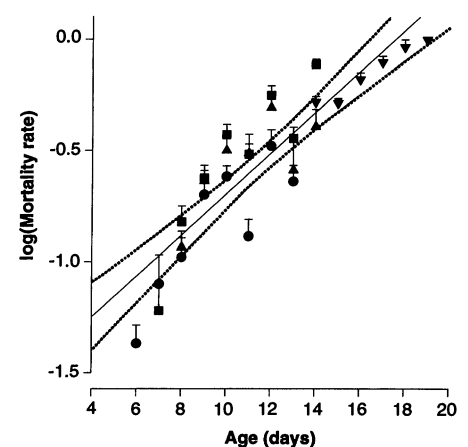
In contrast to these observations, recent

studies (8, 9) have reported that in two insect species—medflies (*Ceratitis capitata*) and the fruit fly (*Drosophila melanogaster*)—mortality rates are not an exponential function of chronological age. In these studies, age-specific mortality rose exponentially for a short period after the emergence of the adult imago but then remained near a high constant level (about 10% mortality per day), or in some cases actually decreased, through the remainder of life. Both studies examined large populations of individuals (up to 1 million medflies), and both argued that exponential increases in mortality in other species are simply an artifact of small population sizes. The

resolution of this argument is important because Gompertzian kinetics have become almost synonymous with “true aging” (4) and because evolutionary models of aging assume a positive relation [not necessarily exponential (10)] between chronological age and mortality rate (11).

We report here that the exponential increase in mortality rate that has been consistently observed in *C. elegans* is not an artifact of small population size. We examined mortality kinetics in *C. elegans* in two ways. First, we assayed survival in 180,000 individuals of a single genotype. To do this, we used a sampling procedure in which a small fraction of the population was analyzed for mortality on each day of life. Second, we analyzed the survival of 1625 hermaphrodites of 79 distinct genotypes that were heterogeneous for mean life-span. These results corroborate our earlier studies, in which mortality rates increased exponentially throughout life in small isogenic populations (5, 6). These analyses also suggest that age-specific mortality rates in genetically heterogeneous populations appear biphasic because they are comprised of subpopulations, each with differing mortality kinetics. Once the subpopulations with the faster rate of increase of mortality have expired, the age-specific mortality rate of the overall population will appear to decelerate, or even decrease, because the only individuals

Fig. 1. Age-specific mortality rates (\pm SEM) of mass cultures of nematodes. A mass culture of TJ1060 [*spe-9(hc88)fer-15(b26)*] was established as described (12). We assessed the mean mortality rate by taking eight subpopulations of approximately 25 worms at each age and monitoring daily mortality over a 3-day period in this smaller population, which was maintained under identical conditions as the mass culture, except for nematode density. Symbols: (●) age-specific mortality first day after subculture, (■) age-specific mortality second day after subculture, and (▲) age-specific mortality third day after subculture. Regressions were performed on mortality for each day of subculture; the slopes of these regression lines were not significantly different ($P = 0.38$) nor were the intercepts ($P = 0.25$) by analysis of variance. The mortality rate of the last 824 nematodes (▼) from the starting population of approximately 180,000 is plotted beginning at 15 days of age. The line shown is the least squares regression ($\pm 95\%$ confidence interval) of mean daily mortality on age [$\log(\text{hazard rate}) = -1.616 + 0.092 \text{ age}$, $r^2 = 0.789$].



A. Brooks and T. E. Johnson, Institute for Behavioral Genetics and Department of Psychology, University of Colorado, Boulder, CO 80309.

G. J. Lithgow, Institute for Behavioral Genetics, University of Colorado, Boulder, CO 80309.

*To whom correspondence should be addressed.